Received: 10 May 2021 | Revised: 31 May 2021 | Accepted: 3 June 2021

DOI: 10.1002/gj.4203

RESEARCH ARTICLE

WILEY

Cambrian marine radial cerebroid ooids: Participatory products of microbial processes

Enzhao Xiao[1] | Muhammad Riaz[2,3,4] | Tehseen Zafar[5] | Khalid Latif[6]

[1]Key Laboratory for Polar Science, MNR, Polar Research Institute of China, Shanghai, China

[2]Centre for Geographical Information System, University of the Punjab, Lahore, Pakistan

[3]State Key Laboratory of Oil and Gas Reservoir Geology and Exploitation, Chengdu University of Technology, Chengdu, China

[4]College of Energy Resources, Chengdu University of Technology, Chengdu, China

[5]Chinese Academy of Sciences, Institute of Geochemistry, Guiyang, China

[6]National Centre of Excellence in Geology, University of Peshawar, Peshawar, Pakistan

Correspondence
Tehseen Zafar, Chinese Academy of Sciences, Institute of Geochemistry, Guiyang 550081, China.
Email: zafar@vip.gyig.ac.cn

Funding information
National Key R&D Program of China, Grant/Award Number: 2019YFC1509102; Shanghai Sailing Program, Grant/Award Number: 21YF1452100

Handling Editor: Z. Lan

The Cambrian Miaolingian Series strata at the Kouquan section, North China, are primarily divided into the Xuzhuang, Zhangxia, and Gushan formations. This particular series comprises oolitic limestone in the middle to upper intervals. Thin section observations of carbonate rock samples from the Zhangxia Formation show that the well-preserved and most remarkable grains among them are cerebroid ooids. Although these ooids have characteristic serrated margins, they are distinct from ooids reported in previous publications due to inconspicuous concentric laminae and radial structures composed of micrite and microspar. To understand the origin of these ooids, we employed petrographic examination, X-ray diffraction (XRD), scanning electron microscopy (SEM), electron probe microanalysis (EPMA), and isotope analyses to explore their compositions and conditions of development. In addition, the occurrence of these cerebroid ooids is closely related to that of dark-coloured micrite: most cerebroid ooids and quasi-cerebroid ooids float inside dark micrite; dark micrite appears in the interior of cerebroid ooids as a radial micrite structure. EPMA and energy-dispersive X-ray (EDX) spectroscopy analyses of micrite reveal that the dark micrite consists of lithomicrobial mats. Fine-scale characterization of the dark micrite inside these cerebroid ooids shows the presence of filamentous and bowl-shaped calcified microbial fossils and extracellular polymeric substance (EPS) calcified remnants. Isotopic data indicate a variation of $\delta^{13}C$ isotopic values between −4.92‰ and −0.11‰ (VPDB) and −9.89‰ and −4.93‰ for $\delta^{18}O$ values (VPDB). The negative values of $\delta^{13}C$ in the studied ooid suggest the genesis of carbon from the high organic-rich zone such as the microbial zone. Also, the ^{13}C-depleted carbon values in the ooids advocate that the carbon is mainly derived from organic sources associated with the sulphate reduction bacterial activity. Thus, isotopic data of this study also provide consistent clues in favour of microbial participation during the genesis of cerebroid ooids. In conclusion, our new findings strongly confirm that the cerebroid ooids of the North China Platform are genetically related to microbial processes.

KEYWORDS
cerebroid ooids, filamentous cyanobacteria, geochemistry, Miaolingian Zhangxia Formation, microbial mat, North China Platform

1 | INTRODUCTION

Since Sorby (1879) recognized that ooid growth is like that of a snowball, the investigation of the ooid formation mechanism, which has more than 100 years of history, has been one of the most intriguing problems in sedimentology (Duguid, Kyser, James, & Rankey, 2010; Flugel & Munnecke, 2010). Previous studies have shown that the following conditions must be satisfied for the formation of ooids: (a) the existence of a nucleus, (b) the orderly renewal of the degassing environment, and (c) the saturation of calcium carbonate in the depositional environment, which is considered a product of physical and chemical processes (Bathurst, 1975; Conley, 1977; Fabricius, 1977; Mei, 2012; Nesteroff, 1956; Simone, 1981; Tucker & Wright, 1990). However, with the development of research on microbial metabolism mediating organomineralization (Reitner, 2004) and the discovery of microorganism contributions to modern (Diaz et al., 2015; Diaz, Eberli, Blackwelder, Phillips, & Swart, 2017) and artificially cultivated (Brehm, Krumbein, & Palinska, 2006) ooid formation, biogenicity has been introduced into the study of ooid genesis (Diaz & Eberli, 2019).

In recent years, studies on the origin of modern ooids (Batchelor, Burne, Henry, Li, & Paul, 2018; Diaz et al., 2015, 2017; Diaz, Piggot, Eberli, & Klaus, 2013; Edgcomb et al., 2013; O'Reilly et al., 2017; Rankey & Reeder, 2011; Reitner, Arp, Thiel, & Galling, 1997; Summons, Bird, Gillespie, Pruss, & Sessions, 2013) and laboratory simulations of oolitic formations (Brehm et al., 2006; Zhou, Zheng, & Zhao, 2017) have shown that microorganisms clearly contribute to ooid formation. In particular, as an explanation for the amorphous calcium carbonates (ACC) within concentric ooids, a conceptual shift from the inorganic precipitate hypothesis (Duguid et al., 2010) to the biological formation of ACC (Diaz et al., 2017) has been achieved. The problem arises while studying the ancient ooids that possibly they change their structure due to diagenesis. Current research has gradually improved the interpretation as well as the possible origin of the ooids with radial structures, especially those from ancient strata.

Current examples and investigations of rock records specify that microbial mats can play a role in forming organic mineral deposits through the interactions among substrates, the water environment, and the atmosphere, which remain multifaceted within sedimentary rocks (Dupraz et al., 2009; Riding, 2000). Beyond this fact, some evidence of biogenicity in ooids from ancient strata has been gradually revealed (Gerdes et al., 1994; Lan & Chen, 2012; Li et al., 2017; Riaz, Xiao, Latif, & Zafar, 2019; Riaz, Zafar, Latif, Xiao, & Ghazi, 2021). These reports indicate that some of the evidence for the formation of marine carbonate ooids in ancient strata can still be preserved in the rock record. In this study, a special kind of cerebroid ooid was observed in oolitic limestone samples from the Cambrian Miaolingian Zhangxia Formation at the Kouquan section, Hebei Province, North China Platform. These cerebroid ooids are distinct from those previously reported due to their inconspicuous concentric laminae and their radial structure. More importantly, the occurrence of these cerebroid ooids is robustly associated with dark micrite inside or around them. We integrated the results from $\delta^{13}C$ and $\delta^{18}O$ isotopes and X-ray diffraction (XRD) to promote the interpretation of the cerebroid ooid–forming environment. Fluorescence microscopy, scanning electron microscopy (SEM), energy-dispersive X-ray (EDX) spectroscopy, and electron probe microanalysis (EPMA) were carried out to assess the ultrastructure and geochemical characteristics of these cerebroid ooids and micrite. The interpretation of the association between cerebroid ooids and micrite can provide innovative insight into the intricate formation of radial structures and open an avenue for further investigation regarding the evidence that microbial communities directly or indirectly participated in ancient ooid formation.

2 | GEOLOGICAL BACKGROUND

Based on structural and geochemical data, the Archean to the Palaeoproterozoic basement of the North China Craton can be separated into three key tectonic units including the Western Block, the Eastern Block, and the Trans-North China Orogen (Lan, Chen, Li, & Kaiho, 2013). Following the formation of the North China Craton during the Lüliangian Orogeny at 2.0–1.8 Ga, the North China Craton experienced a series of extensional and rifting events at 1.8–1.6 Ga which prompted the formation of aulacogens and marginal rift basins. These aulacogens accommodated onshore shallow marine deposits during the transgression phase (Lan et al., 2013 and references therein). The sedimentary rocks in North China are dominated by mainly shallow marine siliciclastics and carbonates. The North China Platform is a stable carbonate platform that developed on the North China Craton (McKenzie, Hughes, Myrow, Choi, & Park, 2011; Mei, 2011; Myrow et al., 2015; Riaz et al., 2019; Rogers & Santosh, 2002; Xiao, Zafar, Latif, Riaz, & Lu, 2019). The North China Platform is characterized by microbially induced sedimentary structures such as wrinkle structures, levelled ripple marks, organic carbonaceous laminae, polygonal sand cracks, polygonal sand crack fills, and gas domes (Lan et al., 2013). After a long period of exposure and denudation during the Archean, the first transgression on the North China Platform commenced from the Late Cambrian Series 2, and the sedimentation was initiated (Mei, 2015; Sun, Yang, Wu, & Wilde, 2012; Ying, Zhou, Su, & Tang, 2011; Zheng, Xiao, & Zhao, 2013). The initial transgression from the southeast of the North China Platform formed an unconformity similar to the 'giant unconformity' of the North American Platform (Lee & Chough, 2011; Meng, Ge, & Tucker, 1997; Myrow et al., 2015). The transgression reached its maximum extent in the Middle Cambrian Zhangxia depositional period, and consequently, the ancient land was developed in the northwest (Kwon, Chough, Choi, & Lee, 2006; Lee & Chough, 2011; Meng et al., 1997; Wu, Zhang, Lu, & Liu, 2017), thus, forming a Cambrian–Ordovician sequence of mixed carbonate-siliceous sedimentary rocks with a thickness of 1800 m (Chough et al., 2010; Meng et al., 1997; Myrow et al., 2015). The east and north of the North China Platform remained submerged during the Middle to the Late Cambrian (Chen, Lee, & Woo, 2014; Meng et al., 1997), contributing to the development of microbiolites.

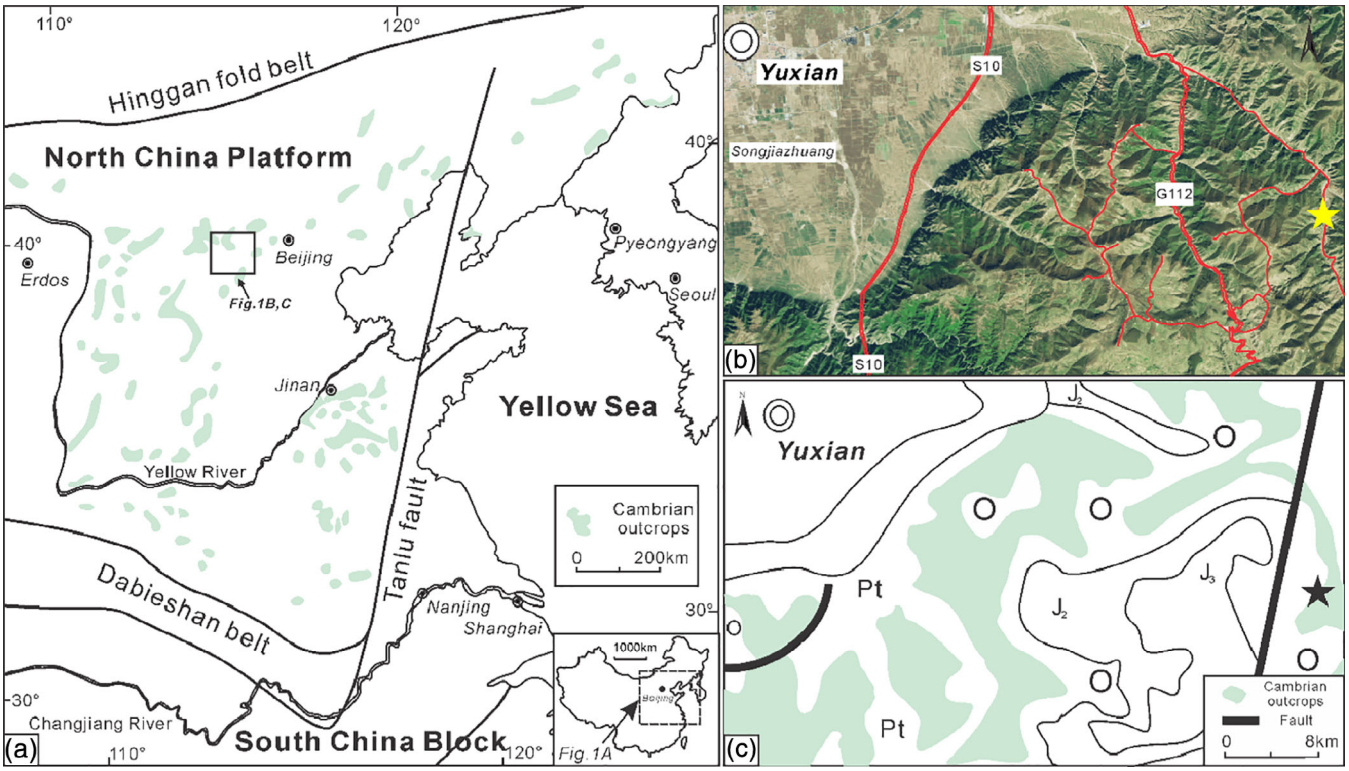

FIGURE 1 Geological setting of the study area. (a) Location of the study area on the North China Platform, (b) satellite map of the survey area (star showing the location of the Kouquan section), and (c) geologic map showing the Cambrian outcrops and the location of the Kouquan section indicated by the star

The studied Kouquan section is located 30 km southeast of Yuxian city and crops out broadly in the middle part of the North China Platform (Figure 1a–c). The Miaolingian Series in the studied section consists of the Xuzhuang, Zhangxia, and Gushan formations (Figure 2a; e.g., Peng & Zhao, 2018). The oolitic-grain bank developed in the upper part of these formations during the relative sea-level fall (see Ma, Mei, Zhang, & Li, 2017; Riaz et al., 2021; Riaz, Xiao, et al., 2019; Riaz, Zafar, Latif, Ghazi, & Xiao, 2020). It is characterized by shallow shelf ooidal shoals, flanked seawards by a ramp, and landwards by tidal flats (e.g., Feng et al., 1990; Feng, Peng, Jin, Jiang, & Bao, 2004; Mei, Riaz, Zhang, Meng, & Hu, 2021). The studied Zhangxia Formation makes conformable lower and upper contacts with the Xuzhuang Formation and Gushan Formation, respectively (Figures 2a,b and 3). The Zhangxia Formation at the Kouquan section is interpreted as three subsequences based on cyclicity of sedimentary facies at different levels (Figure 2a). The lower part of each subsequence is marked by calcareous mudstone of shelf facies (Figures 2b and 3). However, the middle part of each subsequence is characterized as banded mudstone interbedded with thin beds of oolitic limestone (Figure 3). Massive oolitic limestone is noted in the top part of each subsequence together with a thin bed of micrite limestone forming shallow ramp to grain-bank facies (Figures 2 and 3c–f). Variations in the internal lithological characteristics of the Zhangxia Formation reveal changes from non-ooidal to grain bank facies and a shallowing-upward trend in the deposited sediments.

3 | MATERIALS AND METHODS

This study was based on field observations, samples, and measurements of the Cambrian Zhangxia Formation at the Kouquan section (Figure 3). The lithological column of the exposed strata was constructed based on observations from the field and the laboratory (Figure 3). A total of 50 fresh, representative samples of oolitic and micritic limestone were collected from the Zhangxia Formation (Figure 3) and studied from field observations to microstructural examination. Comprehensive microfacies observation analyses (cross-polarized light and plane-polarized light) were conducted on polished samples and thin sections of medium- to thin-bedded oolitic limestone of the second subsequence of the Zhangxia Formation (Figure 2b,c) to illustrate the main lithological and biological components.

SEM studies of the nanofacies were undertaken on polished thin sections and freshly broken surfaces. Samples were gold-coated, depending on whether they were prepared for microanalysis or textural study with SEM. Semiquantitative element analyses of submicron-sized spots during SEM observations were obtained using EDX spectroscopy under a high voltage of 10.0 kV and pulses of 5.45–51.82 kcps.

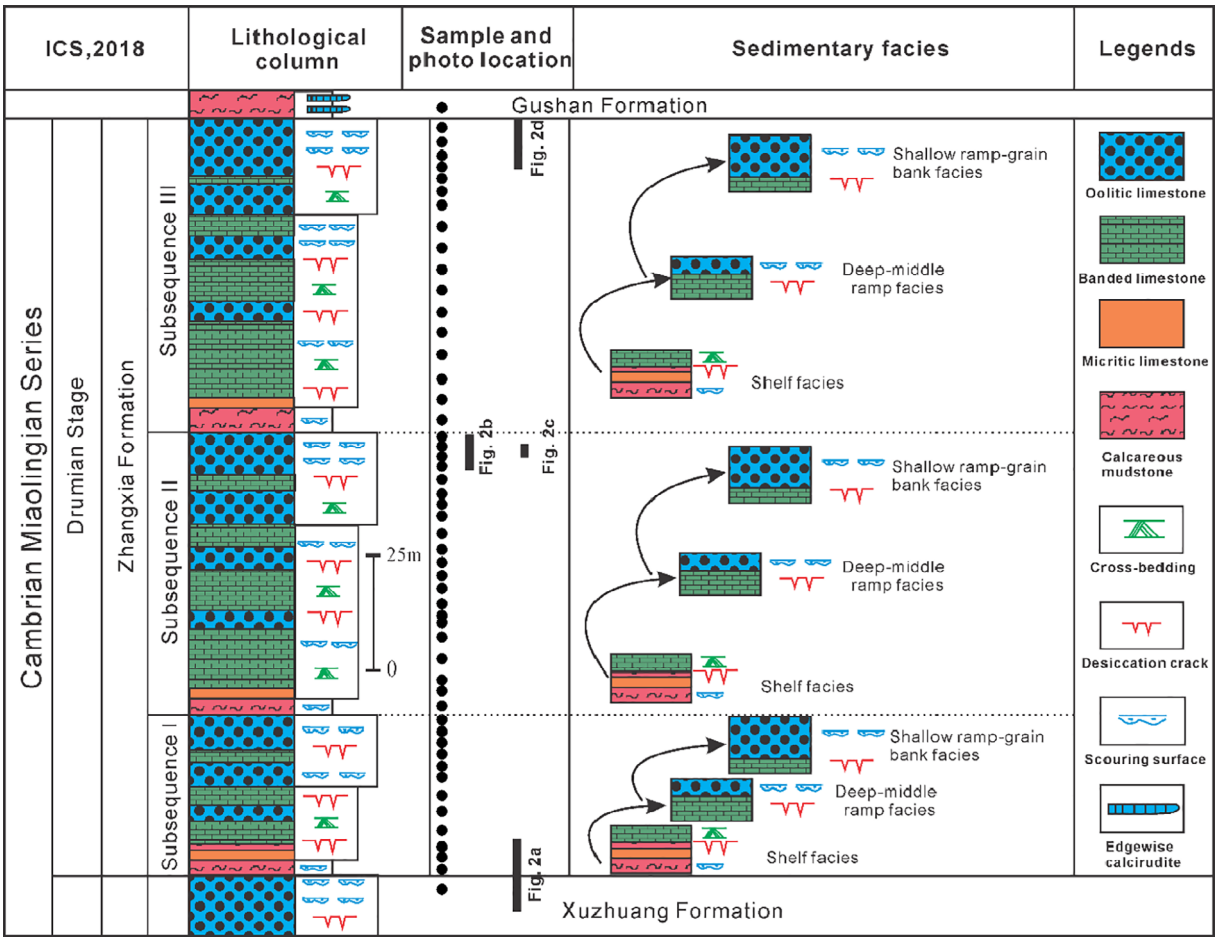

FIGURE 2 Sequence stratigraphic column of the Cambrian Miaolingian Zhangxia Formation at the Kouquan section, North China Platform

Carbon and oxygen isotope analyses were carried out on 21 selected bulk samples that were microdrilled and then dissolved in orthophosphoric acid. These particular samples were also observed under the microscope as lacking calcite veins, which indicate the entire absence of secondary features. Therefore, based on microscopic and field investigations, samples without secondary phenomena were analysed for isotopic assessment. The carbonate isotopic compositions ($\delta^{13}C$ and $\delta^{18}O$) were measured by a Thermo Scientific Delta V Advantage continuous flow isotope ratio mass spectrometer. The results are expressed in delta (d) notation relative to the Vienna Peedee belemnite (V-PDB) standard. The accuracies of the carbon and oxygen isotope ratios for duplicate analyses were within ±0.1‰. In addition, the bulk mineral compositions of 10 representative samples were determined by XRD analyses. Smaller pieces with lengths of 5 mm were cut from the bottoms of four core plugs and then ground into powder. Whole-rock XRD was performed on the prepared powder samples using a Bruker D2 PHASER instrument. Fluorescence microscopic analysis was used to show the strong reactions inside limestone, and EPMA was employed as an experimental method at the microscale to analyse the compositions. All geochemical analyses of oolitic limestone samples were performed in the State Key Laboratory of Oil and Gas Geology and Exploitation, Chengdu University of Technology.

4 | RESULTS

4.1 | Microfacies description of oolitic limestone

Microscale observations show that most of the oolitic limestone samples are little affected by diagenetic modification and that the exquisite structure of oolitic grains is well preserved (Figure 4). The individual sizes of these ooids range between 200 and 600 μm (Figure 4a,b), which are smaller than concentric ooids as described by Riaz, Xiao, et al. (2019); Riaz et al. (2021). Some ooids have distinct nuclei that are approximately 80 μm or more, with regular shapes (Figure 4a,b). These nuclei mainly comprise micritic mud or echinoderm and trilobite fossils (Figure 4a). The neomorphosed ooids were also observed along with radial ooids (Figure 4a–c). These ooids comprise very fine crystals of dolomite (Figure 4c). These grains have probably undergone dissolution of coatings as well as cores and later filing by sparry cement.

The ooids with the radial structures of micrite (Figure 4a–d; red and green arrows) account for overall a larger proportion of the ooids than the ooids with the radial structure of calcite

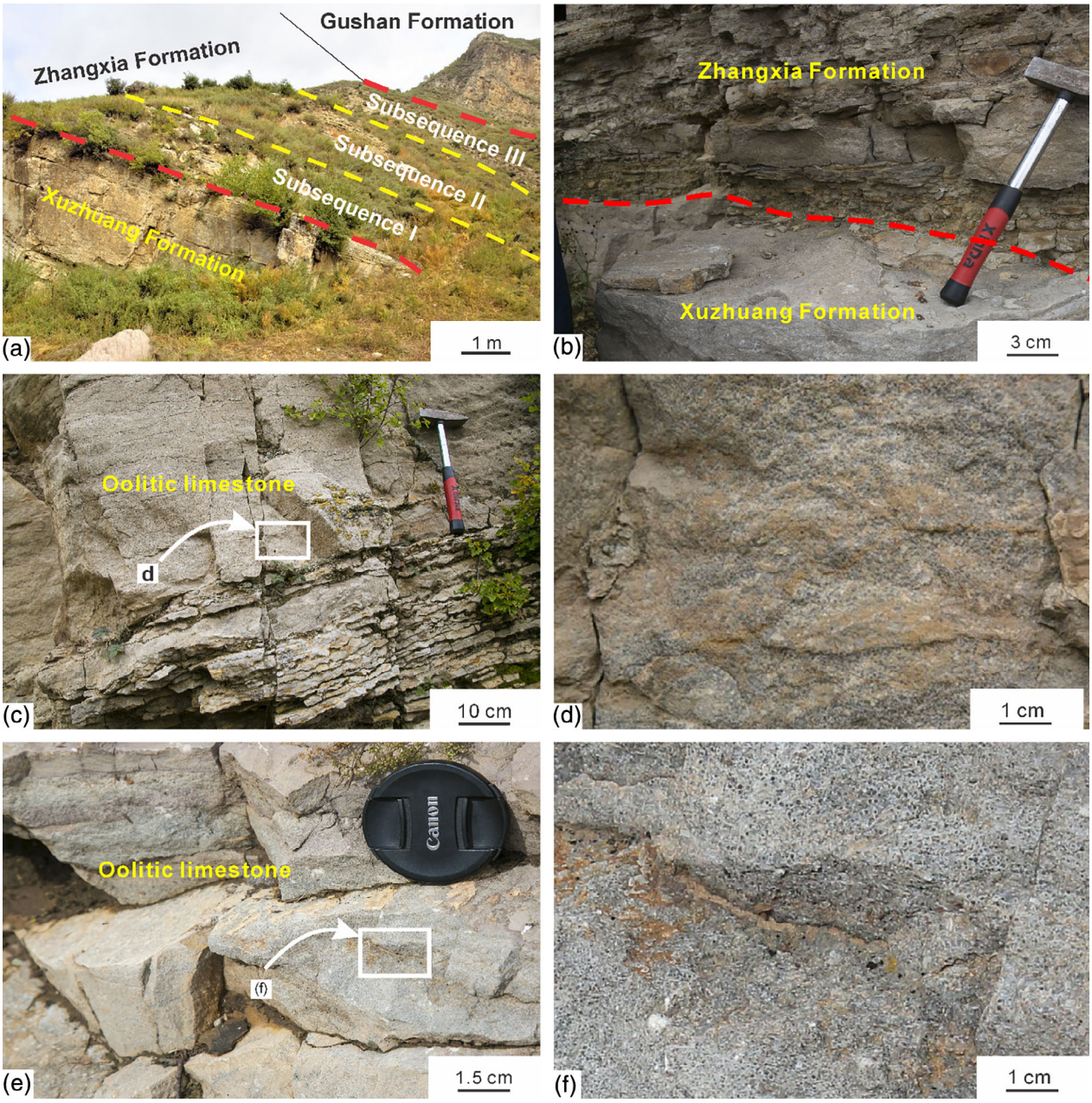

FIGURE 3 Outcrop images showing the lithofacies of the Miaolingian Series strata at the Kouquan section. (a) Contact among Xuzhaung Formation, three subsequences of the Zhangxia Formation, and Gushan Formation, (b) the conformable lower contact of the Zhangxia Formation with the Cambrian Xuzhuang Formation. The calcareous mudstone in the lower part of the Zhangxia Formation makes subsequence I, (c) oolitic limestone in the upper part of subsequence II of the Zhangxia Formation, (d) enlarged part of image c that shows the oolitic limestone, (e) oolitic limestone in the upper part of subsequence III of the Zhangxia Formation, and (f) zoom part of rectangle in image e that represents the oolitic limestone

(Figure 4a,b; yellow arrow) and single crystal ooids (Figure 4a,b; white arrow) of the subsequence II of the Zhangxia Formation. In addition, some small calcite particles are bound by dark micrite, forming individual grains that are smaller and similar to aggregates with radial structures (Figure 4e). These small particle aggregates also have jagged edges in terms of morphology, and dark micrite participates in the main body composition, which may represent the precursors before the formation of the cerebroid ooids. According to the developmental characteristics of the radial structure, radial ooids can be subdivided into two types: (a) in one type, the inner core (the starting point of the radiating structure) is not clear; however, an obvious dark micrite sheath attaches outside of the ooid body and composes the cortex of ooids (Figure 4f) and (b) the other type of radial ooids can be depicted as having circular shapes, jagged edges and smaller sizes than normal ooids based on the microscopic investigation (Figure 4c,d). This kind of ooid used

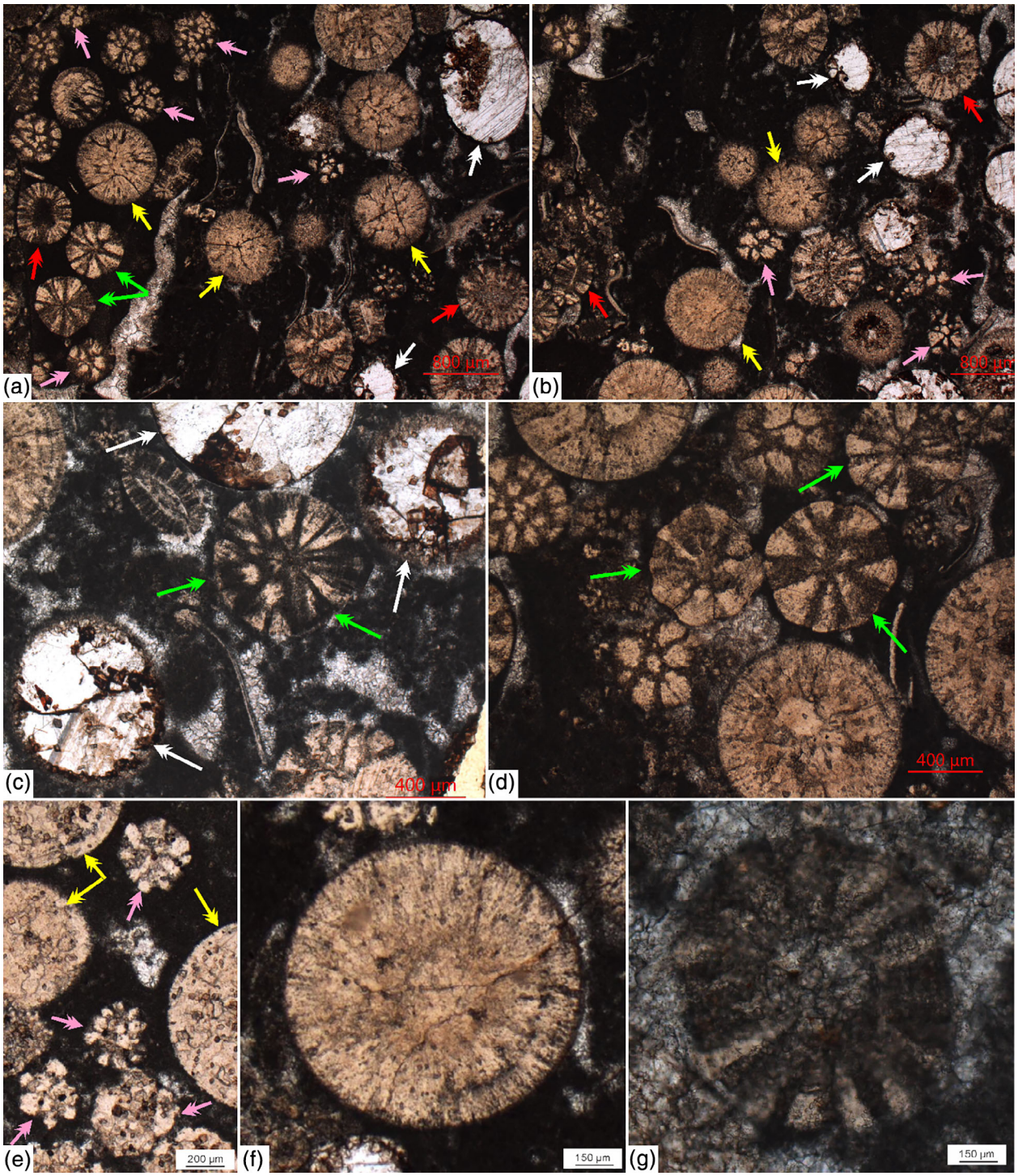

FIGURE 4 (a, b) Radial ooids without core and concentric structure (yellow arrow), the ooids with nuclei of micritic mud or echinoderm and trilobite fossils and radial micrite structure (red arrow), neomorphosed ooids (white arrow), cerebroidal ooids (green arrow), and calcite particle aggregates (pink arrow) with a surrounding matrix of dark and dense micrite forming wackestone of the subsequence II of the Zhangxia Formation, (c) single crystal ooids (white arrow) depict the crystals of dolomite and cerebroid ooids (green arrow) with radial micrite structure, (d) typical cerebroid ooids (green arrow) with radial micrite structure surrounded by dark micrite, (e) alternative structure of radial micrite (yellow arrow) and calcite minerals (pink arrow) show the low-energy setting of their development, (f) radial ooids without concentric structure; and (g) alternating radial layers of dark micrite and white calcite

to be described as cerebroid ooids (see Carozzi, 1962; Flugel & Munnecke, 2010; Wigforss-Lange, 2007). The diameters of these cerebroid ooids range from 100 to 300 μm, and most of them contain radial fabric; however, few varieties reveal inconspicuous concentric layers (Figure 4d). The more interesting feature is that the occurrence of these ooids is intimately associated with dark micrite, which can

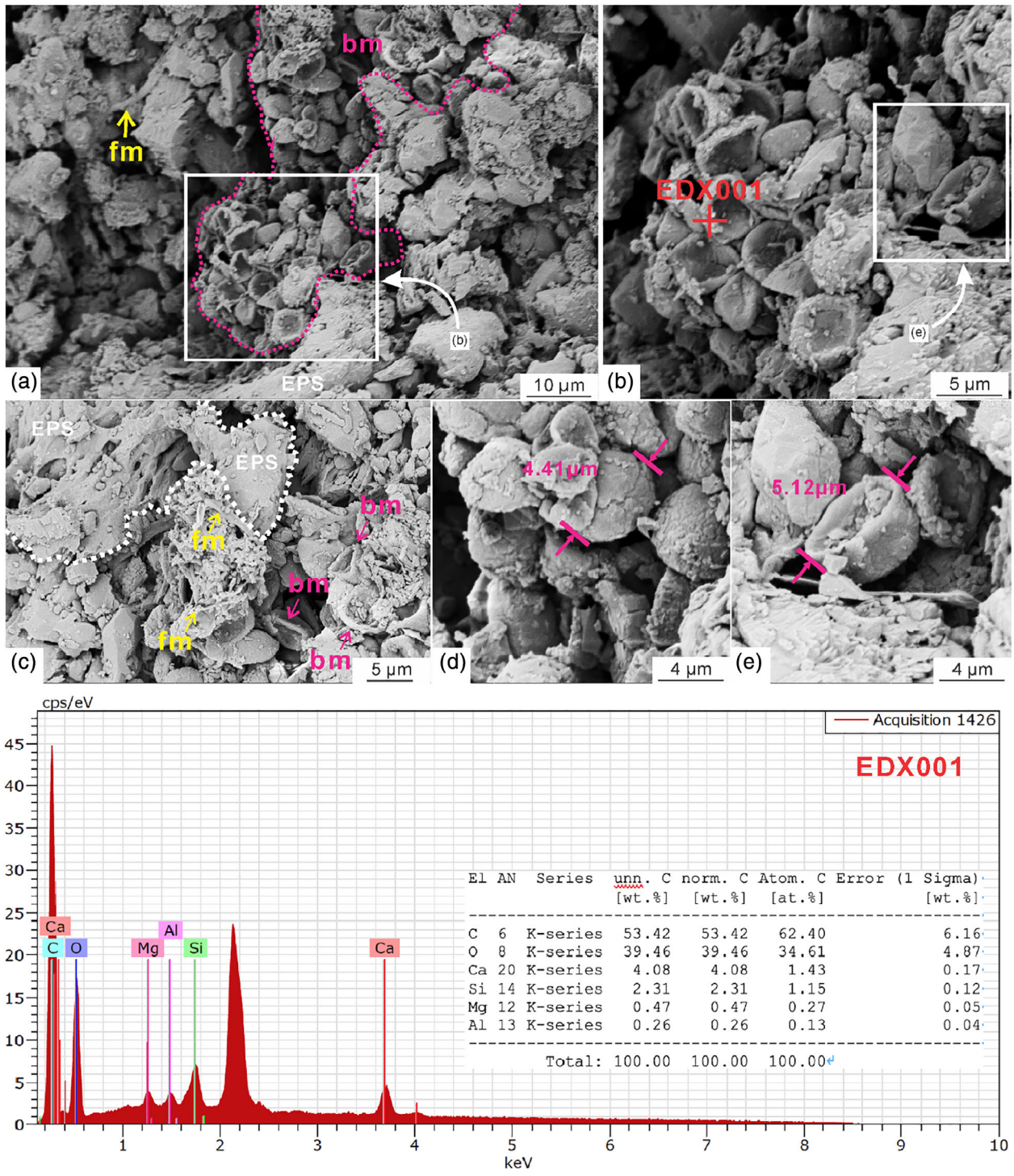

FIGURE 5 Ultra-microfabric and energy-dispersive X-ray (EDX) results for micrite outside and inside the cerebroid ooids, showing bowl-shaped calcified microbial fossils and mineralogy. (a) Bowl-shaped microbial fossil community (bm) (circled by the pink dotted line) inside dark micrite together with filamentous microbial fossils (fm) and extracellular polymeric substance (EPS), (b) Botryoidal aggregate of bowl-shaped microbial fossils with the red cross showing the measuring spot of EDX 001, (c) fm occurring next to a bowl-shaped microbial fossil community; green area shows the EPS calcified remnants, and (d, e) local magnifications of a, showing the diameters of bowl-shaped fossils

be deciphered as follows: (a) the majority of the cerebroid ooids are enclosed by dark micrite (Figure 4d) and (b) as part of the cerebroid ooid, micrite appears in the form of a radial structure and accounts for 50% of the cross-sectional surface (Figure 4c,d,g).

4.2 | Geochemical results

To further investigate the possible intrinsic relationship between the formation of these cerebroid ooids and the dark micrite (Figure 4a–g),

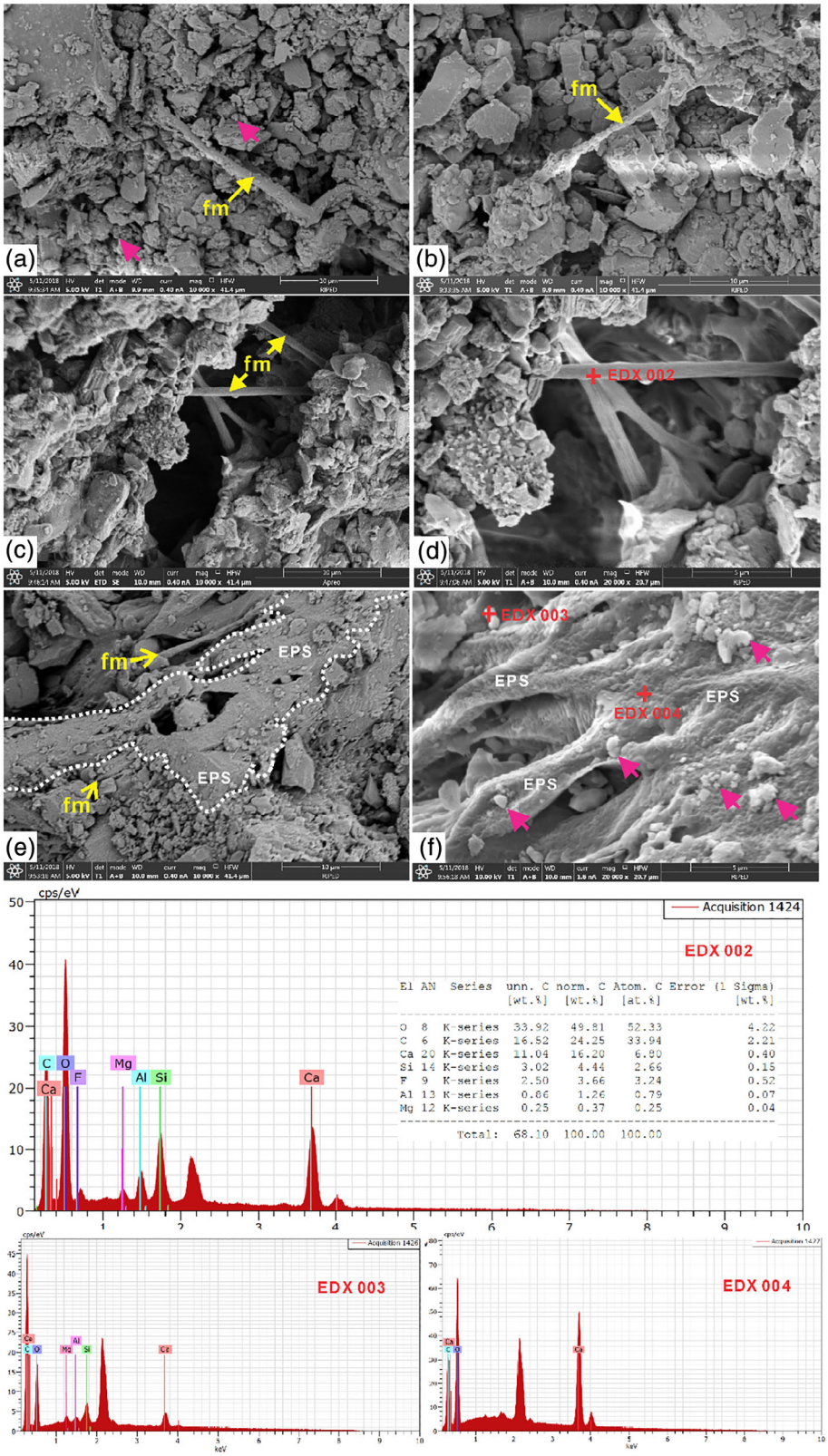

FIGURE 6 Ultra-microfabrics of dark micrite inside and outside the cerebroid ooids, filamentous microbial fossils, nanospheres, EPS-calcified remnants, their aggregates, and EDX results. (a) Type 1 filamentous microbial fossils (fm) inside dark micrite, characterized as individuals that have a single tubular structure with no obvious bifurcations (yellow arrow shows the filamentous microbial fossil (fm); pink arrows indicate nanospheres), (b) type 2 filamentous microbial fossils inside dark micrite; fm marks individuals (pink arrows show nanospheres, and blue arrow shows spherical microbial fossils), (c) type 3 filamentous microbial fossils inside dark micrite; the individual is straight, without obvious bifurcation or distortion, (d) local magnification of (c), red cross showing the target spot of EDX 002, (e) the area inside the green dotted line indicates a large sheet of lamellar EPS-calcified remnants together with several filamentous microbial fossils (fm), (f) EPS-calcified remnants with irregular band-like shapes and ultramicroscopic honeycomb pore structure on the surface; red crosses show the target spots of EDX 003 and EDX 004, and pink arrows show nanospheres. EDX, energy-dispersive X-ray; EPS, extracellular polymeric substance

SEM and EDX were used to observe the ultrastructural features of the dark micrite and the elemental composition of their local ultrastructure. The results showed that these dark micrites do not have an obvious regular mineral crystal structure (Figure 5a). Their complex and irregular ultrastructural features are similar to those of ACC reported in modern ooid research (Batchelor et al., 2018; Diaz et al., 2013, 2015, 2017; Edgcomb et al., 2013; O'Reilly et al., 2017; Summons et al., 2013). In the observation of these dark micrites, nanospheres, extracellular polymeric substance (EPS) calcified remnants and a considerable number of exquisite microbial fossils can be

found. The types of microbial fossils can be classified according to morphology as bowl-shaped microbial fossil communities (Figure 5), curved and intertwined filamentous microbial fossils, and straight and unbranched filamentous microbial fossils (Figure 6).

4.2.1 | Mineral compositions of dark micrite and cerebroid ooids

Under the microscope, we observe that the output of cerebroid ooids is closely related to dark micrite (Figure 5a). To study the genesis of these cerebroid ooids, we attempt to study the mineralogical and geochemical characteristics of these dark micrites based on fluorescence microscopy and EPMA.

Previous studies have shown that calcified biofilm remnants can be preserved inside limestone and exhibit high and bright reflections under fluorescent illumination (Li et al., 2017). Fluorescence microscopic analysis reveals the presence of dark micrite in oolitic limestones from the Zhangxia Formation. Under fluorescence, some parts of dark micrite associated with cerebroid ooids exhibit high and bright reflections (Figure 7b,c), which are the results of the preservation of organic matter remnants.

EPMA analysis was carried out to study the mineral compositions of dark micrite inside and outside the cerebroid ooids and to distinguish the micrite and the radial fibrous calcite of cerebroid ooids. The locations of the microprobe analyses are marked in Figure 7a,d by red crosses (numbered from 1 to 12), and the elemental compositions of micrite and ooid minerals are listed in Table 1. The analysis of the mineral compositions of micrite and cerebroid ooids by EPMA shows that differences in elemental compositions between dark micrite and radial fibrous calcite. The main elements of the cerebroid ooid body are Ca–Mg carbonates (calcite and Mg–calcite; Figure 7, Table 1). By comparison, the micrite is clearly more enriched in a variety of elements such as sulphur, silicon, sodium, potassium, manganese, iron, aluminium, and nitrogen (Figure 7, Table 1), although their main components are carbon, oxygen, and calcium.

XRD analysis was used to observe the basic mineral components (Table 2). The results show that the main composition of the oolitic limestone is calcite, accounting for 90–97%. Small amounts of dolomite appear in some samples, account for 1–5%, and reflect dolomitization. The occurrence of quartz and feldspar shows that terrigenous clasts were mixed during the formation of limestone (Xiao, Wang, Qin, Latif, & Riaz, 2020).

4.2.2 | Carbon and oxygen isotopes

The carbon and oxygen isotope sequences in the middle part of the Zhangxia Formation at the Kouquan section are analysed to infer the possible involvement of microbial mats. Twenty-one groups of oolitic limestone, banded limestone, marl, and mudstone samples from the subsequence II of the Zhangxia Formation were investigated for carbon and oxygen isotope analysis (Table 3). Isotopic data reveal a variation of $\delta^{13}C$ values between −4.92 and −0.11‰ (VPDB) and −9.89‰ and −4.93‰ for $\delta^{18}O$ values (VPDB; Table 3). The test results show that the $\delta^{13}C$ (PDB) values of oolitic limestone and banded limestone are low and negative, that the $\delta^{18}O$ (PDB) values are moderately negative, and that the oxygen isotopes of banded mudstone are lower than those of oolitic limestone. Moreover, the $\delta^{13}C$ (PDB) and $\delta^{18}O$ (PDB) values of both marl and mudstone are highly negative. The increased isotope values of $\delta^{13}C$ and $\delta^{18}O$ in the oolitic limestone indicate that the sedimentary facies most likely formed during a stage of sea-level fall (Figure 8; Spero, Bijma, Lea, & Bemis, 1997; Velivetskaya, Ignatiev, & Gorbarenko, 2009; Zaitsev & Pokrovsky, 2014).

5 | DISCUSSION

5.1 | Ultrastructural and geochemical characteristics of dark micrite inside or outside the cerebroid ooids

The microbial fossils in cerebroid ooids can be classified as bowl-shaped (Figure 5), curved and intertwined filamentous, and straight and unbranched filamentous microbial fossils (Figure 6).

Bowl-shaped microbial fossils occur as clustered communities or botryoidal aggregates (Figure 5a,b), and the original shape of an individual is analogous to a bowl (Figure 5d,e). Some of these fossil individuals are modified by external stresses resulting in bending of edges (Figure 5b,c). The EDX analysis of the bowl-shaped microbial fossils indicates that the main element compositions are carbon and oxygen and that the minor constituent elements are calcium, magnesium, silicon, and aluminium (EDX 001 in Figure 5). The main minerals present may be calcite and clay minerals. However, it is worth noting that the content of carbon is much higher than the content of oxygen. Such an element ratio does not satisfy the carbon requirement for the ratio of carbonate to silicate. This may imply that some of the carbon in the bowl-shaped microbial fossils is preserved in the form of organic carbon. This inference is also consistent with the judgement that the results from fluorescence microscopy also suggest the presence of organic matter inside the dark micrite. In addition, some slab or sheet structures, as well as some filaments, are found near the bowl-shaped microbial fossil communities (Figure 5c). These plate-like or flaky structures most likely reflect EPS calcification (Decho & Gutierrez, 2017; Decho, Visscher, & Reid, 2005; Diaz et al., 2017; Dupraz et al., 2009; Flemming, Thomas, & Daniel, 2007; Lan & Chen, 2012; Lan, Zhang, Tucker, Li, & Zhao, 2020).

In addition to bowl-shaped microorganisms, there are many striking filaments of microbial fossils. Based on the morphological characteristics of filaments, these fossil microorganisms can be subdivided into three types: (a) type 1 bends without bifurcation, and less bending than other types, which seems to be modified by external stresses (Figure 6a), and (b) type 2 filamentous microorganisms have the filaments may be intertwined with each other. The surfaces of filaments are not flat, which can be the product of passive sheath calcification

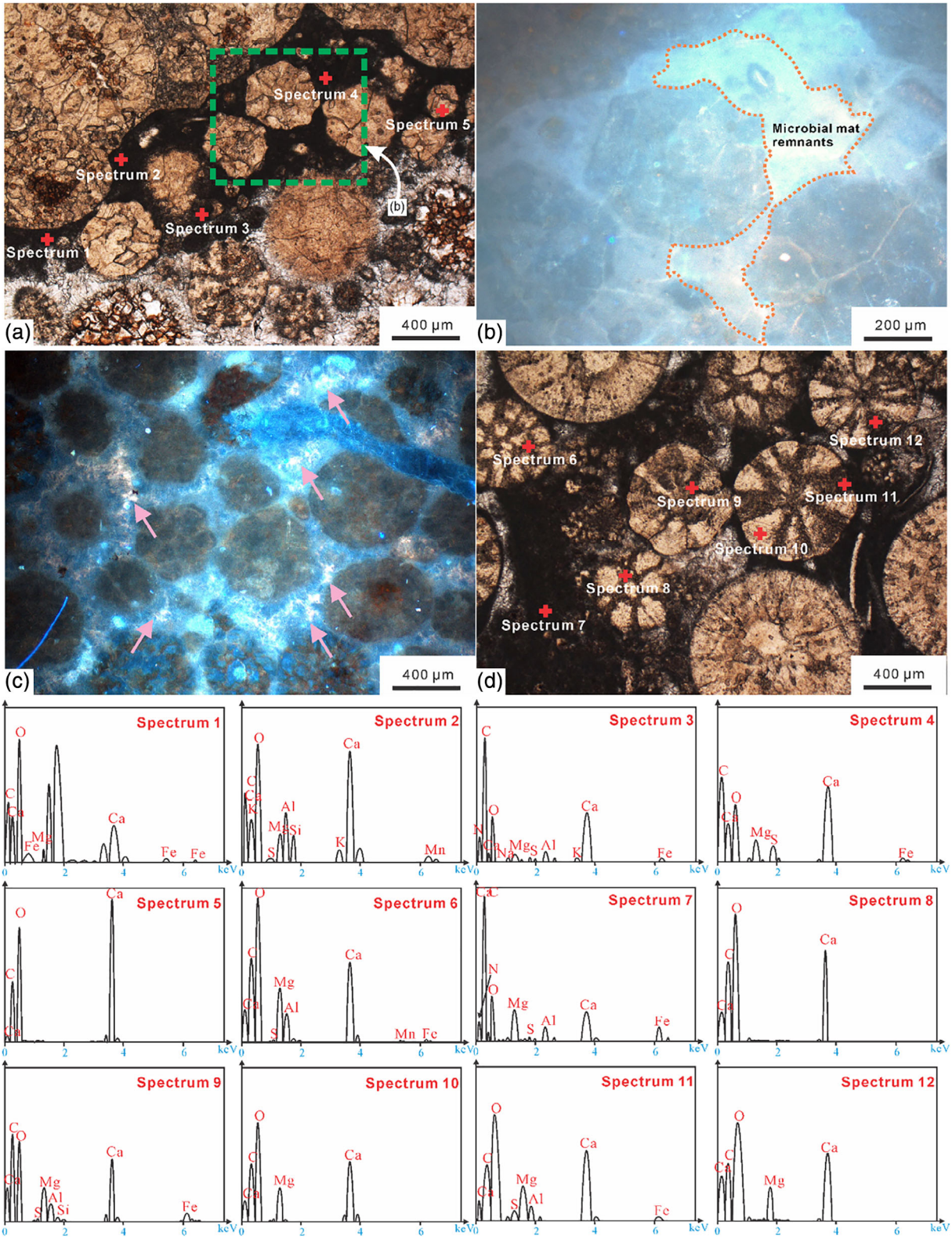

FIGURE 7 Fluorescence photomicrographs, electron probe microanalysis positions, and spectrum results. (a) Typical cerebroid ooids with radial dark micrite inside the ooids with jagged edges and (b) fluorescence microscopic analysis for the local magnification of (a) (shown as the green area). The warm colour of high reflection represents microbial mat remnants; (c) pink arrows indicate high reflection and represent the remnants of organic matter inside the dark micrite surrounding the cerebroid ooids, (d) the polygonal shape of oolitic particles developed in the dark micrite, with sizes much smaller than those of normal ooids. The results for 12 different electron probe microanalysis spots in (a) and (d) are shown at the bottom

TABLE 1 Element compositions of micrite and ooids minerals from electron probe microanalysis

Numbers of spectrum	Spectrum point location	Element compositions of micrite and ooids minerals											
		N_2O_5	SiO_2	SO_3	CO_2	Na_2O	MgO	Al_2O_3	K_2O	CaO	MnO	FeO/FeS	Total
Spectrum 1	Micrite (O-O)				74.55		3.36			18.29		3.8	100%
Spectrum 2	Micrite (O-O)		2.04		52.01	0.36	2.78	6.22	0.26	35.71	0.62		100%
Spectrum 3	Micrite (O-O)	1.97		0.68	61.32	0.57	1.45	2.27	0.33	31.39		0.02	100%
Spectrum 4	Micrite (O-O)			3.12	41.48		5.33			45.26		4.82	100%
Spectrum 5	MB-O				50.28					49.72			100%
Spectrum 6	Micrite (I-O)			0.81	73.38		3.8	2.33		23.03	0.27	0.38	100%
Spectrum 7	Micrite (O-O)	0.65		0.99	63.36		6.51	3.16		22.29		3.04	100%
Spectrum 8	Micrite (I-O)				57.21					42.79			100%
Spectrum 9	Micrite (I-O)		0.37	0.35	56.94		3.97	2.42		36.67		2.12	100%
Spectrum 10	MB-O				52.56		8.9			38.54			100%
Spectrum 11	Micrite (I-O)			1.59	61.05		4.32	1.79		30.54		0.73	100%
Spectrum 12	MB-O				59.65		9.74			30.61			100%

Note: O-O, outside of ooids; I-O, inside of ooids; MB-O, main body of ooids.

TABLE 2 Mineral composition content of oolitic limestone from middle part of Zhangxia Formation

Samples number	Mineral composition content (%)					
	Quartz	Feldspar	Calcite	Dolomite	Pyrite	Clay mineral
KQZX-1	1		94	2	1	2
KQZX-2	1		97	2		
KQZX-3	2		95			3
KQZX-4	1	1	96		1	1
KQZX-5	2		95	3		
KQZX-6	3		92	5		
KQZX-7	1		96	3		
KQZX-8	3		90	5		2
KQZX-9	2		97	1		
KQZX-10	1		97		1	1

of filamentous microorganisms (Figure 6b). (c) Type 3 filamentous fossils do not indicate bending and bifurcation and seldom occur independently (Figure 6c,d). The EDX patterns for type 3 filamentous fossils show the same main element compositions of carbon and oxygen; however, the differences from the bowl-shaped fossils are that (a) in addition to calcium, magnesium, silicon, and aluminium, fluorine occurs inside the microbial fossils and (b) the proportion of oxygen is greater than that of carbon. These contrasts indicate that the different clay mineral components from those of the bowl-shaped fossils and the adequate calcification left no residual organic carbon.

Additionally, several fragmented sheet EPS remnants occur around filamentous microbial fossils (Figure 6e), and large sheet EPS remnants are observed inside the dark micrite together with filamentous microbial fossils and nanospheres (Figure 6e,f). Under the close observation of these EPS lamellae, the surfaces have irregular band-like shapes with an ultramicroscopic honeycomb surficial pore structure (Figure 6f). This characteristic agrees with the basic interpretation of residual calcification of EPSs reported by previous studies, and the composite mineralogical results for nanosphere aggregates represent products from the interaction of heterotrophic bacteria metabolism and the degradation of EPSs (Dupraz et al., 2009; Latif, Xiao, Riaz, & Hussein, 2019; Mei, 2012; Mei et al., 2021; Mei, Latif, Mei, Gao, & Meng, 2020; Mei, Riaz, Wang, Latif, & Zhang, 2020; Xiao, Latif, Riaz, Qing, & Wang, 2018), implying that a preliminary phase of biogenic carbonate particle nucleation was induced by microbial metabolism (Spadafor, Perri, Mckenzie, & Vasconcelos, 2010).

The analytical interpretations of EDX show that these fossils have high elemental concentrations. Calcium, oxygen, and carbon are the main components, while silica and fluorine represent a minor portion, and aluminium and magnesium are very rare (EDX 002 in Figure 6). We can observe high contents of silicon and aluminium and conclude that the main body of the spherical microbial fossils is composed of calcium

TABLE 3 Carbon and oxygen isotopes of the samples from middle part of Zhangxia Formation

Samples number	Lithology	Sedimentary environment	$\delta^{13}C$ (‰) PDB	$\delta^{18}O$ (‰) PDB	*Z*
KQZX-12	Banded limestone	Middle to shallow ramp	−1.62	−5.45	121.27
KQZX-13	Oolitic limestone	Oolitic bank	−0.31	−6.32	123.52
KQZX-14	Oolitic limestone	Oolitic bank	−0.61	−5.63	123.25
KQZX-15	Oolitic limestone	Oolitic bank	−1.49	−6.02	121.25
KQZX-a	Marl	Deep ramp	−2.52	−8.25	
KQZX-b	Mudstone	Shelf	−4.92	−9.89	
KQZX-c	Mudstone	Shelf	−5.33	−9.44	
KQZX-d	Mudstone	Shelf	−4.57	−8.97	
KQZX-1	Oolitic limestone	Oolitic bank	−0.15	−6.99	123.51
KQZX-2	Oolitic limestone	Oolitic bank	−0.57	−6.69	122.80
KQZX-3	Oolitic limestone	Oolitic bank	−0.71	−5.57	123.07
KQZX-4	Oolitic limestone	Oolitic bank	−1.94	−5.51	120.58
KQZX-5	Oolitic limestone	Oolitic bank	−1.39	−5.45	121.74
KQZX-6	Oolitic limestone	Oolitic bank	−0.11	−6.32	123.94
KQZX-A	Oolitic limestone	Oolitic bank	−0.52	−5.63	123.43
KQZX-B	Oolitic limestone	Oolitic bank	−1.49	−6.02	121.25
KQZX-C	Oolitic limestone	Oolitic bank	−0.92	−6.17	122.34
KQZX-D	Banded limestone	Middle to shallow ramp	−1.21	−5.24	122.21
KQZX-E	Banded limestone	Middle to shallow ramp	−0.34	−5.73	123.75
KQZX-F	Oolitic limestone	Oolitic bank	−0.78	−5.22	123.10
KQZX-G	Banded limestone	Middle to shallow ramp	−1.14	−4.93	122.51

carbonate and clay minerals. The EDX analysis of the nanospheres shows that the main elements in the nanospheres are composed of calcium, indicating that the mineral components of these nanospheres are calcium carbonate. Further, EDX analysis of EPS remnants with honeycomb structure suggests that the main components are calcium carbonate and clay minerals (EDX 004 in Figure 6).

5.2 | Interpretation of dark micrite and its genesis in cerebroid ooids

The cerebroid ooids developed in the upper part of the subsequence II of the Zhangxia Formation, during a relative sea-level fall (Figure 3). The cerebroidal ooids comprise the radial structure of dark and dense micrite (Figure 4a–d,g). Further, the surrounding matrix of these ooids is associated with dark micrite (Figure 4a–g). The dark micrite in the studied ooids provide convincing evidence of their microbial genesis that fulfil the studies on modern marine ooids that are genetically correlated with microorganisms (Diaz et al., 2014; Diaz & Eberli, 2019) based on the following features: (a) calcification mediated by microbial activity (Diaz et al., 2014); (b) organic matter entrapped within cortex layers (Folk & Lynch, 2001; O'Reilly et al., 2017); (c) biogeochemical fingerprints (O'Reilly et al., 2017); and (d) high levels of microbial diversity (Diaz et al., 2013, 2014, 2015).

The microscopic features of these samples reveal unique cerebroid ooids with radial structures that are different from those reported in previous studies (Ma et al., 2017; Riaz et al., 2021; Riaz, Xiao, et al., 2019) because their classic concentric laminae are always inconspicuous and most of them are replaced by radial fibre structures with alternating light and dark fibres (Figure 4f). More importantly, the radial cerebroid ooids are strongly associated with dark micrite, as (a) most of them are surrounded by dark micrite and (b) the micritic radial structure inside cerebroid ooids accounts for approximately 50%. Therefore, understanding the origin and source of these dark micrites is the key to interpret the formation of these cerebroid ooids and their special radial structures.

According to previous studies on the origin of micrites, their genesis can be summarized as follows: (a) organic matter (calcium-fixing macromolecules) regulates and participates in or controls biomineralization and the formation of 'organic micrite'; (b) alien microbes and autotrophic microorganisms, as well as metabolic processes, stimulate carbonate precipitation and drive the 'alkalinity engine' that promotes carbonate precipitation in the environment through basic metabolic reactions; and (c) the metabolism of cyanobacteria and algae mediates the conversion of CO_2 into organic carbon compounds, which alters the balance of carbonate solubility in the microenvironment, resulting in the precipitation of carbonates (Edgcomb et al., 2013; Gischler et al., 2017; Guido et al., 2012; Kazmierczak et al., 2015; Mei, 2012; Perry, 1999; Yu et al., 2017). The SEM observations of these dark micrites from the oolitic limestone of the Zhangxia Formation depict nanospheres, EPS-calcified remnants, and diverse kinds of microbial fossils (Figures 5 and 6). The SEM findings for micrite within or around

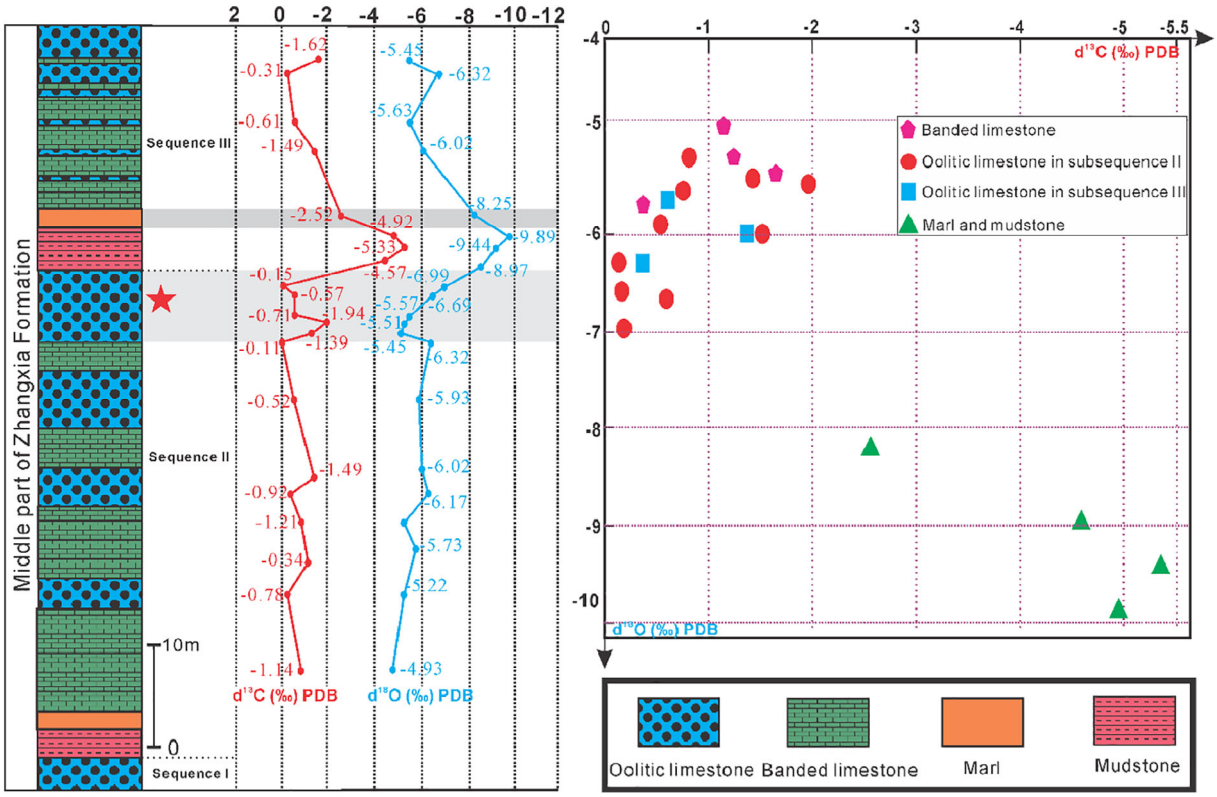

FIGURE 8 Carbon and oxygen isotope sequences in the middle part of the Zhangxia Formation (left) and scatter diagram (right; red star shows the location of the microbial mat, while blue dotted arrows indicate a fourth-order fall in relative sea level)

the cerebroid ooids illustrate a variety of microbial fossils that are identified as bowl-shaped microbial fossil communities (Figure 5a,b), curved and intertwined filamentous microbial fossils (Figure 6a,b), straight and unbranched filamentous microbial fossils (Figure 6c,d), and nanospheres and EPS-calcified remnants (Figure 6c,e,f). The morphological portrayal of these calcified microbial fossils at the ultramicroscale suggests discriminating the metabolic characteristics and taxonomy of these microorganisms is not possible in this study. Nevertheless, they are recognized and confirmed as diverse fossils of microorganisms and communities preserved with dark micrite. The combined diversified element composition results of EPMA and EDX analysis of dark micrite agree with the reported lithification of microbial mats (Dupraz & Visscher, 2005; Farias et al., 2014; Zhu, Lin, Lu, & Dittrich, 2018). These results imply that the dark micrite in oolitic limestone in the Zhangxia Formation reflects calcified remnants of microbial mats with numerous microorganisms (Farias et al., 2014; Zhu et al., 2018). In addition, EPMA data also reveal that the micrite is clearly richer in a variety of elements such as sulphur, silicon, sodium, potassium, manganese, iron, aluminium, and nitrogen (Figure 8, Table 1), although their main components are carbon, oxygen, and calcium. The microzone where nitrogen is present is located inside the dark micrite closely connected with the cerebroid ooids, representing the remnants of organic matter (results of spectra 3 and 7). It is worth noting that the EPMA analysis of dark micrite also reveals the presence of pyrite, which reflects the formation of these dark micrites in a reducing environment and the occurrence of sulphate reduction (Maclean et al., 2010; Xiao et al., 2021; Xiao, Mei, Jiang, & Zafar, 2020; Xiao, Wang, et al., 2020). Combining the finely preserved microbial fossils that we found in the ultramicro features with microbial-related sediments (nanospheres and EPS remnants) and comparing them with those of lithomicrobial mats reported in the literature (Dupraz & Visscher, 2005; Farias et al., 2014; Zhu et al., 2018), we confirm that these dark micrites, which are closely related to radial cerebroid ooids, are lithified microbial mats.

5.3 | Contribution of microbial mats to the formation of cerebroid ooids

Previous studies reported the occurrence of cerebroid ooids in marine or non-marine environments, often coupled with stromatolites (Carozzi, 1962; Wigforss-Lange, 2007). These special grains are characterized by an indented periphery and the mottled appearance of the cortex. The sectors are composed of tangentially arranged laminae and radial micrites which frequently initiate at former depressions on the surface of the nucleus (Flugel & Munnecke, 2010; Summons et al., 2013). However, the radial cerebroid ooids from the Zhangxia Formation are not consistent with stromatolites but are a specific type of ooid.

An important realization was that micrite plays a vital role in these radial cerebroid ooids: almost all cerebroid ooids are wrapped by dark micrite, and inside the cerebroid ooids, micrite appears as part of the

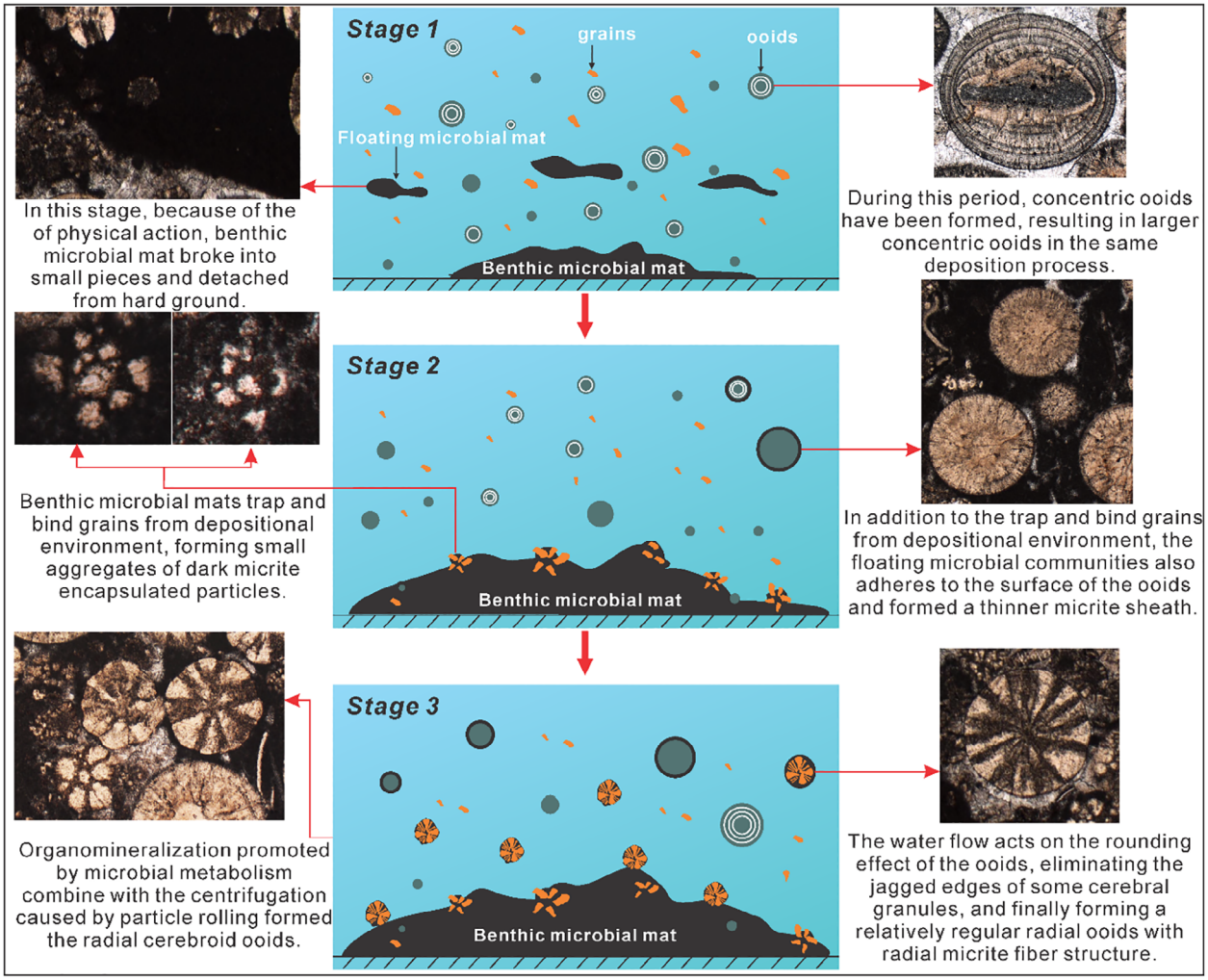

FIGURE 9 Schematic diagrams interpreting the formation processes of radial cerebroid ooids

radial structure. The SEM, EDX, and EPMA results strongly attest that micrites within or outside the radial cerebroid ooids are the remnants of calcified microbial mats. Thus, the microbial mats are confirmed to participate in the formation of cerebroid ooids in three stages: (a) with relative sea-level fall (Figure 2), the shallowing depositional environment (Riaz, Xiao, et al., 2019) leads to an increase in the hydrodynamic influence on the ecological stability of benthic microbial mats. Benthic microbial mats partially fixed on the hard ground are broken into small pieces by the action of waves, tides, or currents (reflected in the irregular dark micrite locally observed within the oolitic limestone; Stage 1 in Figure 9). (b) Microbial communities in suspension maintain biological activity because of EPS protection in a turbulent environment. Some grains are trapped and bounded by benthic microbial mats, which leads to the formation of small grain aggregates (Figure 4g,h). Next, due to the demand for ecological stability, these aggregates adhere to the surfaces of some smaller particles, or microbial communities adhere and capture tiny particles in the turbulent environment (Figure 4e; Stage 2 in Figure 9). (c) These small aggregates of particles form irregular geometries on the benthic microbial mat surface. The shallowing depositional environment causes an increase in hydrodynamic effects (Figure 8). Some of the aggregates are peeled off the microbial mat surface and then form an independent cerebroid ooid. During the formation of cerebroid ooids, complex metabolic effects of the microbial mats (such as sulphate reduction reactions, which can affect carbonate saturation, alkalinity, and pH in the microenvironment), as well as a decrease in microbial communities (EPS degradation and microbial tissue calcification), lead to the formation of the dark micrites (Figures 5 and 6; Stage 3 in Figure 9).

Apart from SEM and EDX confirmations, our isotopic data also provide credible evidence in favour of microbial participation during the genesis of dark micrite in cerebroid ooids. Isotopic data indicate a variation of $\delta^{13}C$ isotopic values between −4.92‰ and −0.11‰ (VPDB) and −9.89‰ and −4.93‰ for $\delta^{18}O$ values (VPDB). The set of $\delta^{13}C$ values is comparable to the feature of marine dissolved organic carbon (Campbell, 2006). First of all, the negative values of $\delta^{13}C$ in the studied ooids reflect that the origin of carbon is predominantly from the high-organic-rich zone, for instance, microbial zone. Secondly, it can also be interpreted that the ^{13}C-depleted carbon values (−4.92 to −0.11‰

VPDB) in the ooids suggest that the carbon is mainly derived from organic sources associated with the sulphate reduction bacterial involvement (Warren, 2000). These $\delta^{13}C$ values of ooids mostly depend on the relative amount of CO_2 which is most likely provided by the decomposition of organic matter linked with the participation of sulphate-reducing bacteria during cementation and recrystallization (e.g., Armstrong-Altrin, Lee, Verma, & Worden, 2009; Wanas, 2002). A number of research works have reported that the negative $\delta^{18}O$ values of several samples can be illuminated by the high degree of recrystallization or owing to meteoric water impact, which reflects that the original values were likely overprinted by the late diagenetic processes (e.g., Campbell, 2006; Campbell et al., 2008). The negative $\delta^{18}O$ values of our samples are not consistent with marine water ambient temperature, however, reflect a most promising influence of diagenetic overprints. This reveals either the effect of surface/near surface during diagenesis (i.e., shallow burial depth). In addition, we report that similar to the oxygen isotope values, the carbon isotope values of most oolitic limestone are higher than those of banded micrite limestone. This difference can be explained by the fact that the low negative values of $\delta^{13}C$ (PDB) most likely suggest that oolitic grains are closely related to microbial communities (as reported in the modern Bahamas; Diaz et al., 2013, 2015, 2017).

6 | CONCLUSIONS

Massive numbers of well-preserved ooids are found in the Zhangxia Formation of the Cambrian Miaolingian Series strata at the Kouquan section that crops out in the central part of the North China Platform. The microscopic characteristics of the remarkable cerebroid ooids from the Zhangxia Formation show that their formation was intimately associated with dark micrite. SEM observations reveal nanospheres, EPS-calcified remnants, and a considerable number of exquisite microbial fossils within the micrite, substantiating that the micrite inside or outside of cerebroid ooids represents the calcified remnants of microbial mats. This hypothesis is confirmed by the EPMA results that the elemental compositions of micrites within or around cerebroid ooids are almost identical to those reported for lithomicrobial mats. In addition, cerebroid ooids and their radial structure can be interpreted as grains in a turbulent marine environment that are trapped and bound by benthic microbial mats, combined with hydrodynamic and microbial-mediated mineralization (calcification). Although from different perspectives, the evidence presented in this research nevertheless confirms that the recent viewpoints on the biogenetic origin of modern ooids are equally applicable to some special oolitic grains in ancient strata.

The negative values of $\delta^{13}C$ in the studied ooid reflect the origin of carbon from the high-organic-rich zone such as the microbial zone. Also, the ^{13}C-depleted carbon values in the ooids suggest that the carbon is mainly derived from organic sources associated with the sulphate reduction bacterial involvement. In summary, our isotopic data provide credible evidence in favour of microbial participation during the genesis of cerebroid ooids. In addition, the negative $\delta^{18}O$ values of several samples reflect a most promising influence of diagenetic overprints.

ACKNOWLEDGEMENTS

The authors gratefully acknowledge Prof. Mingxiang Mei for review of the earlier version of the manuscript. The first author is especially thankful to Dr. Tehseen Zafar for his deep and prolific review, conceptualization, editing, and fairly detailed polishing of the manuscript. This work was supported by the National Key R&D Program of China (2019YFC1509102) and the Shanghai Sailing Program (21YF1452100).

CONFLICT OF INTEREST

The authors declare there is no conflict of interest.

PEER REVIEW

The peer review history for this article is available at https://publons.com/publon/10.1002/gj.4203.

DATA AVAILABILITY STATEMENT

The data that support the findings of this study are available from the corresponding author upon reasonable request.

ORCID

Enzhao Xiao https://orcid.org/0000-0003-3338-2423
Muhammad Riaz https://orcid.org/0000-0002-6154-3354
Tehseen Zafar https://orcid.org/0000-0002-5403-8982
Khalid Latif https://orcid.org/0000-0002-5329-9902

REFERENCES

Armstrong-Altrin, J. S., Lee, Y. I., Verma, S. P., & Worden, R. H. (2009). Carbon, oxygen, and strontium isotope geochemistry of carbonate rocks of the Upper Miocene Kudankulam Formation, Southern India: Implications for paleoenvironment and diagenesis. *Geochemistry*, *69*(1), 45–60.

Batchelor, M. T., Burne, R. V., Henry, B. I., Li, F., & Paul, J. (2018). A biofilm and organomineralisation model for the growth and limiting size of ooids. *Scientific Reports*, *8*, 559. https://doi.org/10.1038/s41598-017-18908-4.

Bathurst, R. G. C. (1975). *Carbonate sediments and their diagenesis* (2nd ed., p. 658). Amsterdam, the Netherlands: Elsevier.

Brehm, U., Krumbein, W. E., & Palinska, K. A. (2006). Biomicrospheres generate ooids in the laboratory. *Geomicrobiology*, *23*, 545–550.

Campbell, K. A. (2006). Hydrocarbon seep and hydrothermal vent paleoenvironments and paleontology: Past developments and future research directions. *Palaeogeography, Palaeoclimatology, Palaeoecology*, *232*, 362–407. https://doi.org/10.1016/j.palaeo.2005.06.018.

Campbell, K. A., Francis, D. A., Collins, M., Gregory, M. R., Nelson, C. S., Greinert, J., & Aharon, P. (2008). Hydrocarbon seep-carbonates of a Miocene forearc (East Coast Basin), North Island, New Zealand. *Sedimentary Geology*, *204*, 83–105. https://doi.org/10.1016/j.sedgeo.2008.01.002.

Carozzi, A. V. (1962). Cerebroid oolites: Transactions of the Illinois State Academy of Science. *Transactions*, *55*(2–3), 239–249.

Chen, J. T., Lee, J. H., & Woo, J. (2014). Formative mechanisms, depositional processes, and geological implications of Furongian (Late Cambrian) reefs in the North China Platform. *Palaeogeography, Palaeoclimatology, Palaeoecology*, *414*, 246–259.

Chough, S. K., Lee, H. S., Woo, J., Chen, J. T., Choi, D. K., Lee, S. B., … Han, Z. Z. (2010). Cambrian stratigraphy of the North China Platform: Revisiting principal sections in Shandong Province, China. *Geosciences Journal*, *14*(3), 235–268.

Conley, C. D. (1977). Origin of distorted ooliths and pisoliths. *Journal of Sedimentary Research*, *47*, 554–564.

Decho, A. W., & Gutierrez, T. (2017). Microbial Extracellular Polymeric Substances (EPSs) in ocean systems. *Frontiers in Microbiology*, *8*, 922.

Decho, A. W., Visscher, P. T., & Reid, R. P. (2005). Production and cycling of natural microbial exopolymers (EPS) within a marine stromatolite. *Palaeogeography, Palaeoclimatology, Palaeoecology*, *219*, 71–86.

Diaz, M. R., & Eberli, G. P. (2019). Decoding the mechanism of formation in marine ooids: A review. *Earth-Science Review*, *190*, 536–556.

Diaz, M. R., Eberli, G. P., Blackwelder, P. L., Phillips, B., & Swart, P. (2017). Microbially mediated organomineralization in the formation of ooids. *Geology*, *45*(9), 771–774.

Diaz, M. R., Piggot, A., Eberli, G., & Klaus, J. (2013). Bacterial community of oolitic carbonate sediments of The Bahamas Archipelago. *Marine Ecology-Progress Series*, *485*, 9–U30.

Diaz, M. R., Swart, P. K., Eberli, G. P., Oehlert, A. M., Devlin, Q., Saied, A., & Altabet, M. A. (2015). Geochemical evidence of microbial activity within ooids. *Sedimentology*, *62*(7), 1–23.

Diaz, M. R., Van Norstrand, J. D., Eberli, G. P., Piggot, A. M., Zhou, J., & Klaus, J. S. (2014). Functional gene diversity of oolitic sands from Great Bahama Bank. *Geobiology*, *12*(3), 231–249.

Duguid, S. M. A., Kyser, T. K., James, N. P., & Rankey, E. C. (2010). Microbes and ooids. *Journal of Sedimentary Research*, *80*(3–4), 236–251.

Dupraz, C., Reid, R. P., Braissant, O., Decho, A. W., Norman, R. S., & Vissher, P. T. (2009). Processes of carbonate precipitation in modern microbial mats. *Earth-Science Reviews*, *96*, 141–162.

Dupraz, C., & Visscher, P. T. (2005). Microbial lithification in marine stromatolites and hypersaline mats. *Trends in Microbiology*, *13*(9), 429–438.

Edgcomb, V. P., Bernhard, J. M., Beaudoin, D., Pruss, S., Welander, P. V., Schubotz, F., … Summons, R. E. (2013). Molecular indicators of microbial diversity in oolitic sands of Highborne Cay, Bahamas. *Geobiology*, *11*, 234–251.

Fabricius, F. H. (1977). Origin of marine ooids and grapestones. *Contributions to Sedimentary Geology*, *7*, 1–113.

Farias, M. E., Contreras, M., Rasuk, M. C., Kurth, D., Flores, M. R., Poire, D. G., … Visscher, P. T. (2014). Characterization of bacterial diversity associated with microbial mats, gypsum evaporites and carbonate microbialites in thalassic wetlands: Tebenquiche and La Brava, Salar de Atacama, Chile. *Extremophiles*, *18*(2), 311–329.

Feng, Z. Z., Peng, Y. M., Jin, Z. K., Jiang, P. L., & Bao, Z. D. (2004). *Lithofacies Palaeogeography of the Cambrian and Ordovician in China* (pp. 1–233). Beijing: Petroleum Industry Press (in Chinese).

Feng, Z. Z., Wang, Y. H., Zhang, J. S., Zuo, W. Q., Zhang, X. L., Hong, G. L., … Yang, C. Y. (1990). *Lithofacies Palaeogeography of the Early Paleozoic of North China Platform* (pp. 1–270). Beijing: Geological Publishing House (in Chinese).

Flemming, H. C., Thomas, R. N., & Daniel, J. W. (2007). The EPS matrix: The "house of biofilm cells". *Journal of Bacteriology*, *189*(22), 7945–7947.

Flugel, E., & Munnecke, A. (2010). *Microfacies of carbonate rocks* (pp. 128–129). Berlin Heidelberg: Springer.

Folk, R. L., & Lynch, L. F. (2001). Organic matter, putative nannobacteria and the formation of ooids and hardgrounds. *Sedimentology*, *48*, 215–229.

Gerdes, G., Dunajtschik-Piewak, K., Riege, H., Taher, A. G., Krumbein, W. E., & Reineck, H. E. (1994). Structural diversity of biogenic carbonate particles in microbial mats. *Sedimentology*, *41*, 1273–1294.

Gischler, E., Heindel, K., Birgel, D., Brunner, B., Reitner, J., & Peckmann, J. (2017). Cryptic biostalactites in a submerged karst cave of the Belize Barrier Reef revisited: Pendant bioconstructions cemented by microbial micrite. *Palaeogeography, Palaeoclimatology, Palaeoecology*, *468*, 34–51.

Guido, A., Vescogni, A., Mastandrea, A., Demasi, F., Tosti, F., Naccarato, A., … Russo, F. (2012). Characterization of the micrite in the late miocenevermetid carbonate bioconstructions, salento peninsula, Italy: Record of a microbial/metazoan association. *Sedimentary Geology*, *263–264*, 133–143.

Kazmierczak, J., Fenchel, T., Kuhl, M., Kempe, S., Kremer, B., Lacka, B., & Malkowski, K. (2015). $CaCO_3$ precipitation in multilayered cyanobacterial mats: Clues to explain the alternation of micrite and sparite layers in calcareous stromatolites. *Life*, *5*, 744–769.

Kwon, Y. K., Chough, S. K., Choi, D. K., & Lee, D. J. (2006). Sequence stratigraphy of the Taebaek Group (Cambrian–Ordovician), mideast Korea. *Sedimentary Geology*, *192*, 19–55.

Lan, Z. W., & Chen, Z. Q. (2012). Scanning electron microscopic imaging and nano-secondary ion microprobe analyses of bacteria-like nanoball structures in oncoids from the Ediacaran Boonall Dolomite of Kimberley, northwestern Australia: Testing their biogenicity. *Carbonates and Evaporites*, *27*, 33–41.

Lan, Z. W., Chen, Z. Q., Li, X. H., & Kaiho, K. (2013). Microbially induced sedimentary structures from the Mesoproterozoic Huangqikou Formation, Helan Mountain region, northern China. *Precambrian Research*, *233*, 73–92.

Lan, Z. W., Zhang, S., Tucker, M., Li, Z., & Zhao, Z. (2020). Evidence for microbes in Early Neoproterozoic stromatolites. *Sedimentary Geology*, *398*, 105589–105592. https://doi.org/10.1016/j.precamres.2013.04.006.

Latif, K., Xiao, E. Z., Riaz, M., & Hussein, A. A. A. (2019). Calcified cyanobacteria fossils from leiolitic bioherm in the Furongian Changshan Formation, Datong (North China Platform). *Carbonates and Evaporites*, *34*(3), 825–843.

Lee, H. S., & Chough, S. K. (2011). Depositional processes of the Zhushadong and Mantou formations (Early to Middle Cambrian), Shandong Province, China: Roles of archipelago and mixed carbonate-siliciclastic sedimentation on cycle genesis during initial flooding of the North China Platform. *Sedimentology*, *58*, 1530–1572.

Li, F., Yan, J. X., Robert, V. B., Chen, Z. Q., Thomas, J. A., Zhang, W., … Xie, S. C. (2017). Paleo-seawater REE compositions and microbial signatures preserved in laminae of Lower Triassic ooids. *Palaeogeography, Palaeoclimatology, Palaeoecology*, *486*, 96–107.

Ma, Y. S., Mei, M. X., Zhang, R., & Li, Y. Y. (2017). Forming patterns for the oolitic bank within the sequence-stratigraphic framework: An example from the Cambrian Series 3 at the Xiaweidian section in the Western Suburb of Beijing. *Acta Petrologica Sinica*, *33*, 1021–1036 (in Chinese with English abstract).

Maclean, L. C., Tyliszczak, T., Gilbert, P. U., Zhou, D., Pray, T. J., Onstott, T. C., & Shoutham, G. (2010). A high-resolution chemical and structural study of framboidal pyrite formed within a low-temperature bacterial biofilm. *Geobiology*, *6*(5), 471–480.

McKenzie, N. R., Hughes, N. C., Myrow, P. M., Choi, D. K., & Park, T. Y. (2011). Trilobites and zircons link north China with the eastern Himalaya during the Cambrian. *Geology*, *39*, 591–594.

Mei, C. J., Riaz, M., Wang, L., Latif, K., & Zhang, R. (2020). Development of Middle Cambrian leiolitic bioherms dominated by calcified microbes: A case study of the Xinji Section (North China Platform). *Marine Micropaleontology*, *157*, 101858. https://doi.org/10.1016/j.marmicro.2020.101858.

Mei, M. X. (2011). Depositional trends and sequence-stratigraphic successions under the Cambrian second-order transgressive setting in the North China Platform: A case study of the Xiaweidian section in the western suburb of Beijing. *Geology in China*, *38*, 317–337 (in Chinese with English abstract).

Mei, M. X. (2012). Brief Introduction on New Advances on the Origin of Ooids. *Acta Sedimentologica Sinica*, *30*(1), 20–32 (in Chinese with English abstract).

Mei, M. X. (2015). Conceptual change from depositional sequences to eustatic sequences: An important development in sequence stratigraphy. *Journal of Stratigraphy*, *39*(1), 58–73 (in Chinese with English abstract).

Mei, M. X., Latif, K., Mei, C. J., Gao, J., & Meng, Q. F. (2020). Thrombolitic clots dominated by filamentous cyanobacteria and crusts of radio-fibrous

calcite in the Furongian Changshan Formation, North China. *Sedimentary Geology*, *395*, 105540. https://doi.org/10.1016/j.sedgeo.2019.105540.

Mei, M. X., Riaz, M., Zhang, Z. W., Meng, Q. F., & Hu, Y. (2021). Diversified calcimicrobes in dendrolites of the Zhangxia Formation, Miaolingian Series (Middle Cambrian) of the North China Craton. *Journal of Palaeogeography*, *10*(8). https://doi.org/10.1186/s42501-021-00087-z.

Meng, X., Ge, M., & Tucker, M. E. (1997). Sequence stratigraphy, sea-level changes and depositional systems in the Cambro-Ordovician of the North China carbonate platform. *Sedimentary Geology*, *114*, 189–222.

Myrow, P. M., Chen, J. T., Snyder, Z., Leslie, S., Fike, D. A., Fanning, C. M., … Tang, P. (2015). Depositional history, tectonics, and provenance of the Cambrian-Ordovician succession in the western margin of the North China Block. *Geological Society of American Bulletin*, *127*, 1174–1193.

Nesteroff, W. D. (1956). La substratum organique dans les depots calcaires, sa signification. *Bulletin de la Société Géologique de France*, *6*(4–5), 381–390.

O'Reilly, S. S., Mariotti, G., Winter, A. R., Newman, S. A., Matys, E. D., Mcdermott, F., … Klepac-Ceraj, V. (2017). Molecular biosignatures reveal common benthic microbial sources of organic matter in ooids and grapestones from Pigeon Cay, The Bahamas. *Geobiology*, *15*, 112–130.

Peng, S. C., & Zhao, Y. L. (2018). The proposed global standard stratotype-section and point (GSSP) for the conterminous base of Miaolingian series and Wuliuan stage at Balang, Jianhe, Guizhou, China was ratified by IUGS. *Journal of Stratigraphy*, *42*(3), 325–327 (in Chinese with English abstract).

Perry, C. T. (1999). Biofilm-related calcification, sediment trapping and constructive micrite envelopes: A criterion for the recognition of ancient grass-bed environments. *Sedimentology*, *46*, 33–45.

Rankey, E. C., & Reeder, S. L. (2011). Holocene oolitic marine sand complexes of The Bahamas. *Journal of Sedimentary Research*, *81*(2), 97–117.

Reitner, J. (2004). Organomineralization: a clue to the understanding of meteoriterelated "bacteria-shaped" carbonate particles. In J. Seckbach (Ed.), *Origins. Genesis, evolution and diversity of life* (pp. 195–212). Dordrecht, the Netherlands: Kluwer Academic Publishers.

Reitner, J., Arp, G., Thiel, V., & Galling, U. (1997). Organic matter in Great Salt Lake ooids (Utah, USA) – First approach to a formation via organic matrices. *Facies*, *36*, 210–219.

Riaz, M., Latif, K., Zafar, T., Xiao, E. Z., Ghazi, S., Wang, L., & Hussein, A. A. A. (2019). Assessment of Cambrian sequence stratigraphic style of the North China Platform exposed in Wuhai division, Inner Mongolia. *Himalayan Geology*, *40*(1), 92–102.

Riaz, M., Xiao, E. Z., Latif, K., & Zafar, T. (2019). Sequence-stratigraphic position of oolitic bank of Cambrian in North China Platform: Example from the Kelan section of Shanxi Province. *Arabian Journal for Science and Engineering*, *44*(1), 391–407.

Riaz, M., Zafar, T., Latif, K., Ghazi, S., & Xiao, E. (2020). Petrographic and rare earth elemental characteristics of Cambrian Girvanella oncoids exposed in the North China Platform: Constraints on forming mechanism, REE sources, and paleoenvironments. *Arabian Journal of Geosciences*, *13*(17), 1–15.

Riaz, M., Zafar, T., Latif, K., Xiao, E. Z., & Ghazi, S. (2021). Cambrian ooids, their genesis and relationship to sea-level rise and fall: A case study of the Qingshuihe section, Inner Mongolia, China. *Stratigraphy*, *18*(2), 139–151. https://doi.org/10.29041/strat.18.2.04.

Riding, R. (2000). Microbial carbonates: The geological record of calcified bacterial-algal mats and biofilms. *Sedimentology*, *47*, 179–214.

Rogers, J. J. W., & Santosh, M. (2002). Configuration of Columbia: A Mesoproterozoic supercontinent. *Gondwana Research*, *5*(1), 5–22.

Simone, L. (1981). Ooids: A review. *Earth Science Review*, *16*, 319–355.

Sorby, H. C. (1879). The structure and origin of limestones. *Proceedings of the Geologic Society of London*, *35*, 56–95.

Spadafor, A., Perri, E., Mckenzie, J. A., & Vasconcelos, C. (2010). Microbial biomineralization processes forming modern Ca: Mg carbonate stromatolites. *Sedimentology*, *57*, 27–40.

Spero, H. J., Bijma, J., Lea, D. W., & Bemis, B. E. (1997). Effect of seawater carbonate concentration on foraminiferal carbon and oxygen isotopes. *Nature*, *390*(6659), 497–500.

Summons, R. E., Bird, L. R., Gillespie, A. L., Pruss, S. B., & Sessions, A. L. (2013). Lipid biomarkers in ooids from different locations and ages: Evidence for a common bacterial flora. *Geobiology*, *11*(5), 420–436.

Sun, J. F., Yang, J. H., Wu, F. Y., & Wilde, S. A. (2012). Precambrian crustal evolution of the eastern North China Craton as revealed by U\Pb ages and Hf isotopes of detrital zircons from the Proterozoic Jing'eryu Formation. *Precambrian Research*, *200*, 184–208.

Tucker, M. E., & Wright, V. P. (1990). *Carbonate sedimentology*. Oxford, England: Blackwell Science.

Velivetskaya, T. A., Ignatiev, A. V., & Gorbarenko, S. A. (2009). Carbon and oxygen isotope microanalysis of carbonate. *Rapid Communications in Mass Spectrometry*, *23*(16), 2391–2397.

Wanas, H. A. (2002). Petrography, geochemistry, and primary origin of spherodial dolomite from the Upper Cretaceous/LowerTertiary Maghra El-Bahari formation at Global Ataqa, northwest Gulf of Suez, Egypt. *Sedimentary Geology*, *151*, 3–4.

Warren, J. (2000). Dolomite: Occurrence, evolution and economically important associations. *Earth-Science Reviews*, *52*, 1–81.

Wigforss-Lange, J. (2007). Tidal facies in the Upper Silurian Öved-Ramsåsa Group of Scania, Sweden: Linkages of radial and cerebroid ooids and evaporite tracers to subtidal, lagoonal environment. *GFF*, *129*, 7–16.

Wu, Y. Y., Zhang, T. S., Lu, J. L., & Liu, Y. (2017). The sedimentological characteristics of microbialites of the Cambrian in the vicinity of Beijing, China. *Journal of Palaeogeography*, *6*(2), 117–131.

Xiao, E., Zafar, T., Latif, K., Riaz, M., & Lu, Y. (2019). Geochemical and petrographic analyses of the Cambrian oncoids of the North China Platform: Implications for their paleogeography and paleoenvironment. *Arabian Journal for Science and Engineering*, *45*(1), 307–325.

Xiao, E. Z., Jiang, S., Zafar, T., Riaz, M., Latif, K., Setoyama, E., … Xin, H. (2021). Sequence stratigraphic and petrological analyses of the Cambrian oncoids exposed in the Liaoning Province, North China Platform. *Australian Journal of Earth Sciences*, 1–19. https://doi.org/10.1080/08120099.2021.1858156.

Xiao, E. Z., Latif, K., Riaz, M., Qing, Y. L., & Wang, H. (2018). Calcified microorganisms bloom in Furongian of the North China Platform: Evidence from Microbialitic-Bioherm in Qijiayu Section, Hebei. *Open Geosciences*, *10*, 250–260.

Xiao, E. Z., Mei, M. X., Jiang, S., & Zafar, T. (2020). Morphology and features of Cambrian oncoids and responses to palaeogeography of the North China Platform. *Journal of Palaeogeography*, *9*(1), 1–18.

Xiao, E. Z., Wang, H., Qin, Y. L., Latif, K., & Riaz, M. (2020). Sedimentary fabrics and environmental characteristics of leiolite in Cambrian: A case study from Changshan Formation in Laiyuan City, Hebei Province. *Acta Sedimentologica Sinica*, *38*(1), 76–90.

Ying, J. F., Zhou, X. H., Su, B. X., & Tang, Y. J. (2011). Continental growth and secular evolution: Constraints from U–Pb ages and Hf isotope of detrital zircons in Proterozoic Jixian sedimentary section (1.8–0.8 Ga), North China Craton. *Precambrian Research*, *189*, 229–238.

Yu, F., Fu, X. G., Xu, G., Wang, Z. W., Chen, W. B., Zeng, S. Q., … Li, X. R. (2017). Geochemical, palynological and organic matter characteristics of the Upper Triassic Bagong Formation from the North Qiangtang Basin, Tibetan Plateau. *Palaeogeography, Palaeoclimatology, Palaeoecology*, *515*, 23–33. https://doi.org/10.1016/j.palaeo.2017.12.002.

Zaitsev, A., & Pokrovsky, B. (2014). Carbon and oxygen isotope compositions of Lower-Middle Ordovician carbonate rocks in the northwestern Russian platform. *Lithology & Mineral Resources*, *49*(3), 272–279.

Zheng, Y. F., Xiao, W. J., & Zhao, G. (2013). Introduction to tectonics of China. *Gondwana Research*, *23*, 1189–1206.

Zhou, G., Zheng, R., & Zhao, G. (2017). Characteristics, origin and geological signifcance of Oncoids of Givetian (Middle Devonian) in Ganxi Area, Northwestern Sichuan. *Journal of Jilin University*, *47*(2), 405–417 (in Chinese with English abstract).

Zhu, T. T., Lin, Y. C., Lu, X. C., & Dittrich, M. (2018). Assessment of cyanobacterial species for carbonate precipitation on mortar surface under different conditions. *Ecological Engineering*, *120*, 154–163.

How to cite this article: Xiao, E., Riaz, M., Zafar, T., & Latif, K. (2021). Cambrian marine radial cerebroid ooids: Participatory products of microbial processes. *Geological Journal*, *56*(9), 4627–4644. https://doi.org/10.1002/gj.4203